

M. AYGUN

Department of Physics, Bitlis Eren University
(Bitlis, Turkey; e-mail: murata.25@gmail.com)

A COMPREHENSIVE RESEARCH OF ^{10}C NUCLEUS USING DIFFERENT THEORETICAL APPROACHES

UDC 539

We perform an extensive theoretical analysis of ^{10}C nucleus with the use of various theoretical approaches involving the different nuclear potentials and different density distributions, as well as a simple cluster approach. We try to explain new measured and challenging experimental data on the $^{10}\text{C} + ^{58}\text{Ni}$ system at 35.3 MeV. First, we investigate the effect of thirteen different potentials. Then, we examine ten different types of density distributions for ^{10}C nucleus. Finally, we present a simple calculation method for various cluster states of ^{10}C , compare all the theoretical results with the experimental data, and obtain their improved agreement.

Keywords: nuclear potential, proximity potential, density distribution, cluster model, elastic scattering, optical model, double folding model.

1. Introduction

The element carbon (C) has 15 isotopes. Among them, ^{12}C (98.93%) and ^{13}C (1.07%) are stable, and ^{14}C is a radionuclide [1]. ^{10}C , which has $J^\pi = 0^+$, $T_{1/2} = 19.308$ s and only one excited state with $J^\pi = 2^+$ and $T_{1/2} = 107$ fs ($E_{2^+} = 3353.7$ keV) [1], is a proton-rich nucleus, and is supposed as only nucleus with the Brunnian (super-Borromean) structure because of the four-body configuration [2,3]. Thus, it can be said that ^{10}C is one of the interesting isotopes of the element carbon.

Recently, Guimarães *et al.* [3] experimentally measured the elastic scattering angular distributions of $^{10}\text{C} + ^{58}\text{Ni}$ reaction at $E_{\text{Lab}} = 35.3$ MeV. They examined the experimental data using the approaches of coupled channels (CC), coupled reaction channels (CRC), and continuum discretized coupled channels (CDCC). In the CC calculations, they applied the São Paulo (SP) potential for the real part and the Woods–Saxon (WS) potential for the imaginary one. They realized that CC calculations were insufficient in defining the experimental data, and the theoretical results need to be improved. For this, they made a progress in the theoretical results, by including the spin reorientation in their CC calculations. However, the need to harmonize the theoretic

cal results in order to fit the experimental data continues. In the CRC calculations, they investigated the effect of transfer reactions on the theoretical results. With this goal, they analyzed one-proton, one-neutron, and two-neutron transfer reactions. In the calculations, they used the SP potential for the real part and the WS potential for the imaginary one. They reported that the CRC calculations with the transfer reactions had a little effect on the elastic scattering results. Finally, they performed the CDCC calculations to improve the agreement between experimental data and theoretical results. Despite all these troublesome and comprehensive theoretical calculations, it was emphasized that theoretical results should be improved. This deficiency induced us to consider carefully the agreement between different theoretical approaches and the elastic scattering experimental data for the ^{10}C projectile.

In the present study, we aim to advance the results of previous study [3] in describing the experimental data by using three different theoretical approaches. First, we obtain the elastic scattering cross-sections of the $^{10}\text{C} + ^{58}\text{Ni}$ reaction for thirteen types of nuclear potentials. Second, we acquire the scattering cross-sections of the $^{10}\text{C} + ^{58}\text{Ni}$ reaction for ten different density distributions of ^{10}C nucleus. Third, we obtain the elastic scattering cross-sections using a simple calculation approach for three different clus-

ter states of ^{10}C nucleus. By comparing the experimental data and all the theoretical results, we offer alternative nuclear potentials, alternative density distributions, and a simple cluster calculation for the $^{10}\text{C} + ^{58}\text{Ni}$ reaction.

Section 2 presents the theoretical method. Section 3 defines the potentials applied in the calculations. Section 4 shows the density distributions of the projectile and the target. Section 5 gives a simple calculation procedure for cluster structures of ^{10}C . Section 6 provides the theoretical results and discussion. Section 7 indicates the summary and conclusions for all the approaches.

2. Theoretical Method

The calculations are performed by using the optical model (OM) that consists of the real and imaginary potentials. The real potential is obtained according to the nuclear potential, density distribution, and cluster structure of the nucleus, the methods being explained below. On the other hand, the imaginary potential is assumed as

$$W(r) = \frac{W_0}{\left[1 + \exp\left(\frac{r-r_w (A_P^{1/3} + A_T^{1/3})}{a_w}\right)\right]}, \quad (1)$$

where W_0 , r_w , a_w , and $A_{P(T)}$ are the depth, radius, diffuseness, and mass of the projectile(target), respectively. So, the total interaction potential can be expressed as

$$V_{\text{total}}(r) = V_{\text{Nuclear}}(r) + V_{\text{Coulomb}}(r), \quad (2)$$

where the $V_{\text{Coulomb}}(r)$ potential [4] is

$$V_{\text{Coulomb}}(r) = \frac{1}{4\pi\epsilon_0} \frac{Z_P Z_T e^2}{r}, \quad r \geq R_c, \quad (3)$$

$$= \frac{1}{4\pi\epsilon_0} \frac{Z_P Z_T e^2}{2R_c} \left(3 - \frac{r^2}{R_c^2}\right), \quad r < R_c, \quad (4)$$

$$R_c = 1.25 (A_P^{1/3} + A_T^{1/3}). \quad (5)$$

In the calculations of the density distributions, the real potentials are calculated by using the double folding model given by

$$V(\mathbf{r}) = \int d\mathbf{r}_1 \int d\mathbf{r}_2 \rho_P(\mathbf{r}_1) \rho_T(\mathbf{r}_2) \nu_{NN}(\mathbf{r} - \mathbf{r}_1 + \mathbf{r}_2), \quad (6)$$

where $\rho_{P(T)}(\mathbf{r}_{1(2)})$, respectively, are the density distributions of the projectile and target nuclei which are explained in Section 4, and ν_{NN} is the effective nucleon-nucleon interaction parametrized by [4] as

$$\nu_{NN}(r) = 7999 \frac{\exp(-4r)}{4r} - 2134 \frac{\exp(-2.5r)}{2.5r} + 276 \left(1 - 0.005 \frac{E_{\text{Lab}}}{A_P}\right) \delta(r) \text{ MeV}. \quad (7)$$

3. Proximity Potentials

The nuclear potential is one of the most significant quantities in the analysis of nuclear interactions, and is still one of the hottest topics in the field of nuclear physics [5–8]. As a result, we are looking for alternative nuclear potentials to analyze the $^{10}\text{C} + ^{58}\text{Ni}$ reaction. For this purpose, we examine thirteen types of the proximity potential summarized in the following section.

3.1. Prox 77, Prox 79, Mod-Prox-88, Prox 2003-I, Prox 2003-II, Prox 2010

Prox 77 potential [9, 10] can be written as

$$V_N^{\text{Prox 77}}(r) = 4\pi\gamma b C_\mu \Phi\left(\zeta = \frac{r - C_p - C_t}{b}\right) \text{ MeV}, \quad (8)$$

where

$$C_\mu = \frac{C_p C_t}{C_p + C_t}, \quad C_i = R_i \left[1 - \left(\frac{b}{R_i}\right)^2 + \dots\right], \quad b \approx 1 \text{ fm}, \quad (9)$$

$$R_i = 1.28 A_i^{1/3} - 0.76 + 0.8 A_i^{-1/3} \text{ fm} \quad (i = p, t). \quad (10)$$

The surface energy coefficient, γ , is assumed to be

$$\gamma = \gamma_0 \left[1 - k_s \left(\frac{N - Z}{N + Z}\right)^2\right]. \quad (11)$$

The universal function, $\Phi(\zeta)$, is accepted as

$$\Phi(\zeta) = \begin{cases} -\frac{1}{2}(\zeta - 2.54)^2 - \\ -0.0852(\zeta - 2.54)^3 \text{ for } \zeta \leq 1.2511, \\ -3.437 \exp\left(-\frac{\zeta}{0.75}\right) \text{ for } \zeta \geq 1.2511. \end{cases} \quad (12)$$

Many studies were carried out on proximity potentials, and different versions were proposed. Except for γ_0 and k_s values of these derived potentials, other parameters are the same as for the Prox 77 potential. The γ_0 and k_s values of proximity potentials investigated in this study are listed in Table 1.

3.2. Broglia and Winther 1991 (BW 91)

BW 91 potential [17] is taken as [18]

$$V_N^{\text{BW 91}}(r) = -\frac{16\pi R_\mu \gamma a}{\left[1 + \exp\left(\frac{r-R_0}{a=0.63}\right)\right]} \text{ MeV}, \quad (13)$$

where

$$R_\mu = \frac{R_p R_t}{R_p + R_t}, \quad R_0 = R_p + R_t + 0.29, \quad (14)$$

$$R_{p,t} = 1.233A_{p,t}^{1/3} - 0.98A_{p,t}^{-1/3}, \quad (15)$$

$$\gamma = 0.95 \left[1 - 1.8 \left(\frac{N_p - Z_p}{A_p} \right) \left(\frac{N_t - Z_t}{A_t} \right) \right]. \quad (16)$$

3.3. Aage Winther (AW 95)

The parameters of AW 95 potential are the same as the BW 91 potential [18, 19] except for the following ones:

$$a = \frac{1}{1.17 \left[1 + 0.53(A_p^{-1/3} + A_t^{-1/3}) \right]}, \quad (17)$$

and

$$R_0 = R_p + R_t, \quad R_{p,t} = 1.2A_{p,t}^{1/3} - 0.09. \quad (18)$$

3.4. Akyuz-Winther (AW)

AW potential [20] is shown by [21]:

$$V_N^{\text{AW}}(r) = V_0 R_\mu \exp \left[\frac{(r - R_p - R_t)}{d} \right] \text{ MeV}, \quad (19)$$

where

$$V_0 = -65.4 \text{ MeV}, \quad R_{p,t} = (1.20A_{p,t}^{1/3} - 0.35) \text{ fm}, \quad (20)$$

$$d = \frac{1}{1.16 \left[1 + 0.48(A_p^{-1/3} + A_t^{-1/3}) \right]} \text{ fm}. \quad (21)$$

Table 1. γ_0 and k_s values of Prox 77, Prox 79, Mod-Prox 88, Prox 2003-I, Prox 2003-II, Prox 2010 potentials

Potential type	γ_0 , MeV/fm ²	k_s	Ref.
Prox 77	0.9517	1.7826	[11]
Prox 79	1.2402	3.0	[12]
Mod-Prox-88	1.65	2.3	[13]
Prox 2003-I	1.08948	1.9830	[14]
Prox 2003-II	0.9180	0.7546	[14]
Prox 2010	1.460734	4.0	[10, 15, 16]

3.5. Christensen and Winther 1976 (CW 76)

CW 76 potential [22] is the same as the AW potential except for the following parameters [10]:

$$V_0 = -50, \quad d = 0.63, \quad R_{p,t} = 1.233A_{p,t}^{1/3} - 0.978A_{p,t}^{-1/3}. \quad (22)$$

3.6. Bass 1980 (Bass 80)

Bass 80 potential is parametrized as [17, 18]

$$V_N^{\text{Bass 80}}(s) = -R_\mu \phi(s = r - R_p - R_t) \text{ MeV}, \quad (23)$$

where

$$\phi(s) = \left[0.033 \exp\left(\frac{s}{3.5}\right) + 0.007 \exp\left(\frac{s}{0.65}\right) \right]^{-1}, \quad (24)$$

$$R_{p,t} = R_s \left(1 - \frac{0.98}{R_s^2} \right), \quad R_s = 1.28A_{p,t}^{1/3} - 0.76 + 0.8A_{p,t}^{-1/3}. \quad (25)$$

3.7. Ngô 1980 (Ngo 80)

Ngô 80 potential was formulated by [23]:

$$V_N^{\text{Ngo 80}}(r) = C_\mu \phi(s = r - C_p - C_t) \text{ MeV}, \quad (26)$$

$$R_{p,t} = \frac{[N(1.1375 + 1.875 \times 10^{-4} A_{p,t}) + (1.128Z)] A_{p,t}^{1/3}}{A_{p,t}}, \quad (27)$$

$$\Phi(s) = \begin{cases} -33 + 5.4(s - s_0)^2 & \text{for } s < s_0, \\ -33 \exp\left[-\frac{1}{5}(s - s_0)^2\right] & \text{for } s \geq s_0, \\ s_0 = -1.6 \text{ fm.} \end{cases} \quad (28)$$

3.8. Denisov (D)

D potential can be shown as [18, 24]

$$V_N^{\text{D}}(r) = -1.989843 R_\mu \phi(s = r - R_1 - R_2 - 2.65) \times \left[1 + 0.003525139 \left(\frac{A_1}{A_2} + \frac{A_2}{A_1} \right)^{3/2} - 0.4113263 (I_1 + I_2) \right] \text{ MeV}, \quad (29)$$

where

$$I_i = \frac{N_i - Z_i}{A_i}, \quad (30)$$

$$R_i = R_{ip} \left(1 - \frac{3.413817}{R_{ip}^2} \right) + 1.284589 \left(I_i - \frac{0.4A_i}{A_i + 200} \right), \quad (31)$$

$$R_{ip} = 1.24A_i^{1/3} \left(1 + \frac{1.646}{A_i} - 0.191 \left(\frac{A_i - 2Z_i}{A_i} \right) \right), \quad (32)$$

$$\phi(s) = \begin{cases} 1 - \frac{s}{0.7881663} + 1.229218s^2 - 0.2234277s^3 - \\ - 0.1038769s^4 - R_\mu(0.1844935s^2 + \\ + 0.07570101s^3 + (I_1 + I_2)(0.04470645s^2 + \\ + 0.0334687s^3)) \quad (-5.65 \leq s \leq 0), \\ \left(1 - s^2 \left(0.05410106R_\mu \exp \left(-\frac{s}{1.76058} \right) - \right. \right. \\ \left. \left. - 0.539542(I_1 + I_2) \exp \left(-\frac{s}{2.424408} \right) \right) \right) \times \\ \times \exp \left(-\frac{s}{0.7881663} \right) \quad (s \geq 0) \quad (i = 1, 2). \end{cases} \quad (33)$$

4. Densities

Another very useful factor in the description of nuclear interactions is the density distribution of nuclei. In this respect, many studies were carried out [25–30]. We are looking for alternative density distributions to explain the nuclear interactions with ^{10}C . In this way, we analyze ten type density distributions of ^{10}C nucleus.

4.1. Density distributions of ^{10}C projectile

4.1.1. Variational Monte Carlo (VMC)

The first density of ^{10}C nucleus was acquired by means of the VMC calculations [31].

4.1.2. Ngô–Ngô (Ngo)

Ngo density can be expressed by [23, 32]

$$\rho_i(r) = \frac{\rho_{0i}}{1 + \exp \left(\frac{r-C}{0.55} \right)}, \quad \rho_{0n(0p)} = \frac{3}{4\pi} \frac{N(Z)}{Ar_{0n(0p)}^3}, \quad (34)$$

where

$$r_{0n} = 1.1375 + 1.875 \times 10^{-4}A, \quad r_{0p} = 1.128 \quad (i = n, p). \quad (35)$$

$$C = R \left(1 - \frac{1}{R^2} \right), \quad R = \frac{(Nr_{0n} + Zr_{0p})A^{1/3}}{A}. \quad (36)$$

4.1.3. Gupta 1 (G1)

G1 density can be displayed as [33, 34]

$$\rho_i(r) = \frac{\rho_{0i}}{1 + \exp \left(\frac{r-R_{0i}}{a_i} \right)}, \quad \rho_{0i} = \frac{3A_i}{4\pi R_{0i}^3} \left(1 + \frac{\pi^2 a_i^2}{R_{0i}^2} \right)^{-1}, \quad (37)$$

$$R_{0i} = 0.90106 + 0.10957A_i - 0.0013A_i^2 + 7.71458 \times 10^{-6}A_i^3 - 1.62164 \times 10^{-8}A_i^4, \quad (38)$$

$$a_i = 0.34175 + 0.01234A_i - 2.1864 \times 10^{-4}A_i^2 + 1.46388 \times 10^{-6}A_i^3 - 3.24263 \times 10^{-9}A_i^4. \quad (39)$$

4.1.4. Gupta 2 (G2)

Differences between G2 and G1 densities are in R_{0i} and a_i values written by [35]

$$R_{0i} = 0.9543 + 0.0994A_i - 9.8851 \times 10^{-4}A_i^2 + 4.8399 \times 10^{-6}A_i^3 - 8.4366 \times 10^{-9}A_i^4, \quad (40)$$

$$a_i = 0.3719 + 0.0086A_i - 1.1898 \times 10^{-4}A_i^2 + 6.1678 \times 10^{-7}A_i^3 - 1.0721 \times 10^{-9}A_i^4. \quad (41)$$

4.1.5. São Paulo (SP)

SP density is described as [36]

$$\rho_i(r) = \frac{\rho_{0i}}{1 + \exp \left(\frac{r-R_i}{a_i} \right)} \quad (i = n, p) \quad (42)$$

where

$$R_n = 1.49N^{1/3} - 0.79, \quad R_p = 1.81Z^{1/3} - 1.12, \quad (43)$$

$$a_n = 0.47 + 0.00046N, \quad a_p = 0.47 - 0.00083Z. \quad (44)$$

4.1.6. Fermi 1 (F1)

F1 density has the same form with SP outside of $R_{n(p)}$ and $a_{n(p)}$ parameters given by [37]

$$R_n = 0.953N^{1/3} + 0.015Z + 0.774, \quad (45)$$

$$a_n = 0.446 + 0.0072 \left(\frac{N}{Z} \right),$$

$$R_p = 1.322Z^{1/3} + 0.007N + 0.022,$$

$$a_p = 0.449 + 0.0071 \left(\frac{Z}{N} \right). \quad (46)$$

4.1.7. Fermi 2 (F2), Fermi 3 (F3), Fermi 4 (F4), Fermi 5 (F5)

F2, F3, F4, and F5 densities are in the 2pF density form, and their parameters are listed in Table 2.

4.2. Target nucleus density

^{58}Ni density of the target nucleus in the reaction under study takes the following form:

$$\rho(r) = \frac{\rho_0}{1 + \exp\left(\frac{r-c}{z}\right)}, \quad (47)$$

where $\rho_0 = 0.172$, $c = 4.094$ and $z = 0.54$ [42].

5. Simple Cluster Approach

Recently, a simple cluster approach was applied to ^9Li [43], ^9Be [44], ^{12}Be [45], and ^{22}Ne [46] nuclei. With this goal, we investigate $^6\text{Be} + \alpha$, $^9\text{B} + p$ and $^8\text{Be} + 2p$ cluster structures indicated for ^{10}C in the literature, by using a simple cluster approach.

5.1. $^6\text{Be} + \alpha$

The ^{10}C density in the $^6\text{Be} + \alpha$ cluster structure [3] can be written as

$$\rho^{10\text{C}}(r) = \rho^{6\text{Be}}(r) + \rho_{\alpha}(r), \quad (48)$$

where the ^6Be density is obtained by using G1 approach, and the α density is taken as [4]

$$\rho_{\alpha}(r) = 0.4229 \exp(-0.7024r^2). \quad (49)$$

5.1.1. $^9\text{B} + p$

The ^{10}C density for the $^9\text{B} + p$ cluster structure [3] is assumed as

$$\rho^{10\text{C}}(r) = \rho^{9\text{B}}(r) + p, \quad (50)$$

where the ^9B density is produced via G1 approach, and the proton density is taken as [47, 48]

$$\rho_p(r) = \left(\frac{1}{\gamma\sqrt{\pi}}\right)^3 \exp(-r^2/\gamma^2). \quad (51)$$

5.1.2. $^8\text{Be} + 2p$

Finally, the ^{10}C density for the $^8\text{Be} + 2p$ cluster structure [49] is in the following form:

$$\rho^{10\text{C}}(r) = \rho^{8\text{Be}}(r) + 2p, \quad (52)$$

where the ^8Be density is determined with G1 approach, and the proton density has the same form as Eq. (51).

6. Results and Discussion

6.1. Comparison of nuclear potentials

To present the effect of various potentials in explaining the elastic cross-sections of the $^{10}\text{C} + ^{58}\text{Ni}$ system, we investigated thirteen type potentials such as Prox 77, Prox 79, Mod-Prox-88, Prox 2003-I, Prox 2003-II, Prox 2010, BW 91, AW 95, AW, CW 76, Bass 80, Ngo 80 and D. First, we calculated the potentials by using the FORTRAN code developed by us. The variations with the distance of the potentials are demonstrated in Fig. 1. Then, the cards FRESKO over the obtaining values were generated. The imaginary potential was accepted to have the WS shape. To achieve convenient results with the data, the parameters W_0 , r_w , and a_w of the WS potential were changed at intervals of 0.1 and 0.01 fm and were listed in Table 3. The theoretical calculations based on the OM were performed by using the code FRESKO [51].

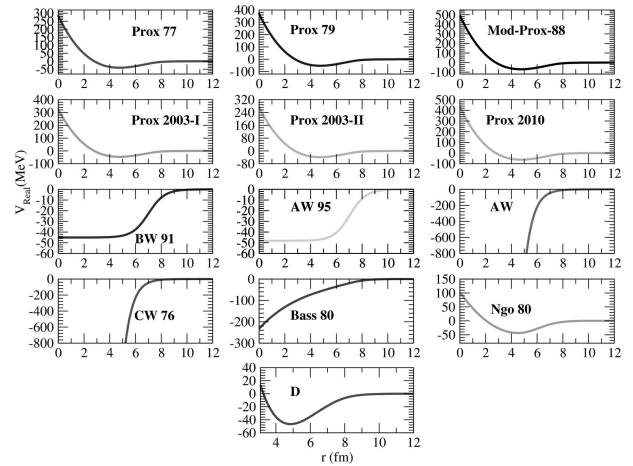


Fig. 1. Changes with the distance of the real potentials such as Prox 77, Prox 79, Mod-Prox 88, Prox 2003-I, Prox 2003-II, Prox 2010, BW 91, AW 95, AW, CW 76, Bass 80, Ngo 80 and D

Table 2. ρ_0 , R_0 and a values of F2, F3, F4, and F5 density distributions

Density	ρ_0	R_0	a	Ref.
F2	0.126414	$1.07A^{1/3}$	0.54	[38]
F3	$\rho_{0n} = 0.0808$ $\rho_{0p} = 0.0929$	$R_{0n} = 1.96$ $R_{0p} = 2.16$	$a_{0n} = 0.469$ $a_{0p} = 0.499$	[39]
F4	$\frac{0.212}{1+2.66A^{-2/3}}$	$1.04A^{1/3}$	0.54	[40]
F5	0.16	$1.15A^{1/3}$	0.50	[41]

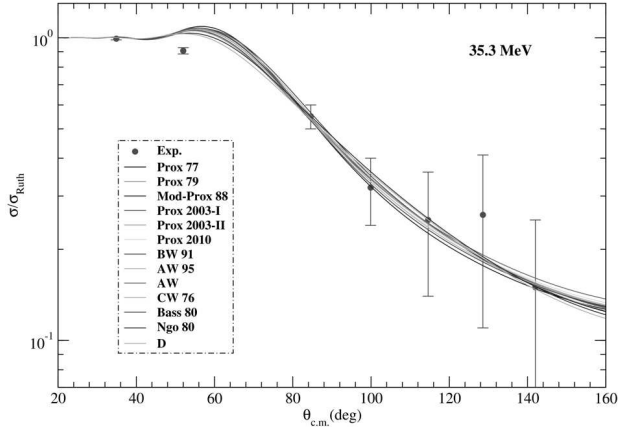


Fig. 2. The elastic scattering cross-sections calculated by using Prox 77, Prox 79, Mod-Prox 88, Prox 2003-I, Prox 2003-II, Prox 2010, BW 91, AW 95, AW, CW 76, Bass 80, Ngo 80 and D potentials [3]

We calculated the elastic scattering cross-section of the $^{10}\text{C} + ^{58}\text{Ni}$ reaction at $E_{\text{Lab}} = 35.3$ MeV for thirteen various nuclear potentials and presented the results, as compared with the experimental data, in Fig. 2. In this respect, we observed that the results of Prox 2003-I and Prox 2003-II potentials are very similar to each other. We note that a similar situation is valid for the results of Prox 77 and Prox 79 po-

Table 3. The WS parameters and χ^2/N values obtained by using Prox 77, Prox 79, Mod-Prox 88, Prox 2003-I, Prox 2003-II, Prox 2010, BW 91, AW 95, AW, CW 76, Bass 80, Ngo 80 and D potentials

Potential type	W_0 , MeV	r_w , fm	a_w , fm	χ^2/N
Prox 77	32.9	1.42	0.326	1.63
Prox 79	30.9	1.42	0.302	1.59
Mod-Prox 88	33.9	1.40	0.280	2.04
Prox 2003-I	32.9	1.42	0.315	1.59
Prox 2003-II	32.9	1.42	0.327	1.59
Prox 2010	30.9	1.42	0.285	1.62
BW 91	26.5	1.42	0.280	1.63
AW 95	32.9	1.42	0.280	1.69
AW	34.9	1.42	0.280	1.51
CW 76	30.3	1.42	0.280	1.60
Bass 80	32.9	1.42	0.280	1.80
Ngo 80	32.9	1.42	0.350	1.58
D	32.0	1.42	0.380	1.60

Table 4. The rms radii for VMC, Ngo, G1, G2, SP, F1, F2, F3, F4, F5, $^6\text{Be} + \alpha$, $^9\text{B} + \text{p}$ and $^8\text{Be} + 2\text{p}$ together with the literature data

Density/Cluster	rms
VMC	2.431
Ngo	2.578
G1	2.200
G2	2.195
SP	2.304
F1	2.529
F2	2.686
F3	2.425
F4	2.653
F5	2.671
$^6\text{Be} + \alpha$	1.749
$^9\text{B} + \text{p}$	2.478
$^8\text{Be} + 2\text{p}$	2.739
Literature data	2.55 ^a , 2.44 ^b , 2.51 ^c 2.27 ± 0.03 ^d , 2.42 ± 0.1 ^e

^a The antisymmetrized molecular dynamics (AMD) [39].

^b HF+BCS with the SIII effective interaction [39].

^c HF+BCS with the SLy4 effective interaction [39].

^d From experiment in Ref. [50]. ^e From Ref. [39].

tentials. We deduced that the AW result was slightly better than the other results, when all the results were compared with one another. So, we can suggest AW potential as an alternative potential for the analysis of the $^{10}\text{C} + ^{58}\text{Ni}$ reaction.

6.2. Comparison of density distributions

The theoretical analysis of the elastic scattering cross-section of the $^{10}\text{C} + ^{58}\text{Ni}$ system was also performed for ten different densities of ^{10}C nucleus including VMC, Ngo, G1, G2, SP, F1, F2, F3, F4, and F5. The root mean square (rms) values corresponding to the densities are listed together with the literature data in Table 4.

The real potentials were obtained for ten various densities within the double folding model (DFM) based on the OM. However, the imaginary potential for all the density calculations was taken in the WS type. The parameters W_0 , r_w and a_w of WS potential were examined at 0.1 and 0.01 step intervals, and the values were shown in Table 5. The code DF POT [52] for the DFM calculations and the code FRESCO [51] for the OM calculations were used.

Figure 3 demonstrates the change with r (fm) of ten various densities of the ^{10}C projectile. G2 density has the highest density in the center part, while VMC density displays the lowest density in the center. Some densities are different in the center part, whereas their tails are similar.

Figure 4 provides the elastic scattering cross-section of the $^{10}\text{C} + ^{58}\text{Ni}$ reaction at an incident energy of 35.3 MeV. It is seen that the densities present a close behavior to one another. In this sense, G1, G2 and F3 results are very close to one another, especially G1 and G2 results. At the same time, it has been noticed that the consistency with the experimental data of G1, G2, and F3 densities over the comparative analysis of all the results is better than the results of other densities. Additionally, it can be said that F3 result is very slightly better than G1 and G2 results within the scope of the error value ($\frac{\chi^2}{N}$).

Figure 5 displays the change with r (fm) of the real potentials of VMC, Ngo, G1, G2, SP, F1, F2, F3, F4, and F5 densities. It is seen that G1 and G2 densities are deeper than the other densities, and F2 density is the shallowest one.

Jouanne *et al.* [39] examined the sensitivity to the rms value of elastic scattering cross-sections. In this context, they stated that the calculations with the rms radius 2.42 ± 0.1 fm gave more compatible results with the elastic scattering data. This rms value (2.42 ± 0.1 fm) corresponds to F3 density (2.425 fm) in

Table 5. The normalization constant (N_R), WS parameters and $\frac{\chi^2}{N}$ values for the calculations with VMC, Ngo, G1, G2, SP, F1, F2, F3, F4, and F5 densities

Density type	N_R	W_0 , MeV	r_w , fm	a_w , fm	$\frac{\chi^2}{N}$
VMC	1.00	30.3	1.42	0.24	1.69
Ngo	0.83	33.9	1.42	0.23	1.81
G1	1.00	33.9	1.42	0.29	1.63
G2	1.00	33.9	1.42	0.29	1.62
SP	1.00	33.9	1.42	0.27	1.67
F1	0.93	32.9	1.42	0.24	1.79
F2	0.70	32.9	1.42	0.24	1.69
F3	0.73	33.9	1.42	0.29	1.59
F4	0.81	34.9	1.42	0.23	1.94
F5	0.80	33.9	1.42	0.23	1.83

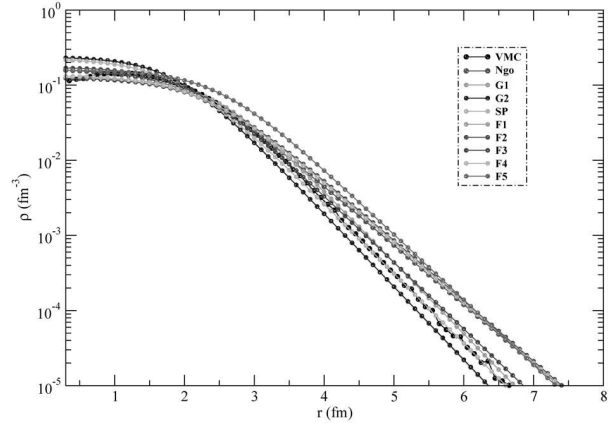


Fig. 3. Changes with the distance of VMC, Ngo, G1, G2, SP, F1, F2, F3, F4, and F5 densities of ^{10}C nucleus on the logarithmic scale

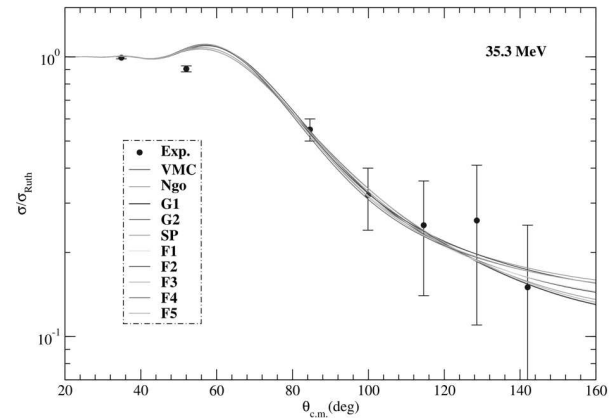


Fig. 4. The elastic cross-sections calculated by using VMC, Ngo, G1, G2, SP, F1, F2, F3, F4, and F5 densities [3]

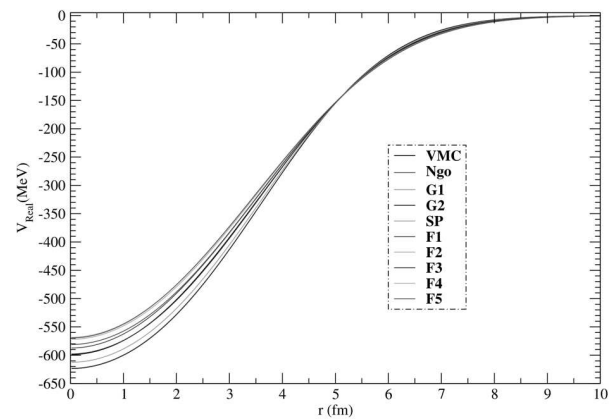


Fig. 5. Changes with the distance of the real potentials calculated by using VMC, Ngo, G1, G2, SP, F1, F2, F3, F4, and F5 densities

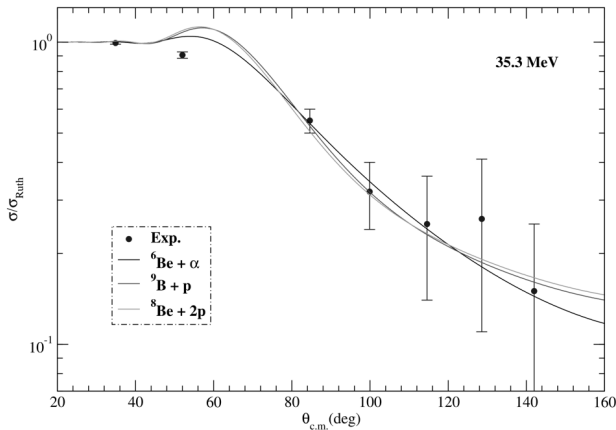


Fig. 6. The elastic cross-sections acquired via ${}^6\text{Be} + \alpha$, ${}^9\text{B} + p$ and ${}^8\text{Be} + 2p$ cluster structures [3]

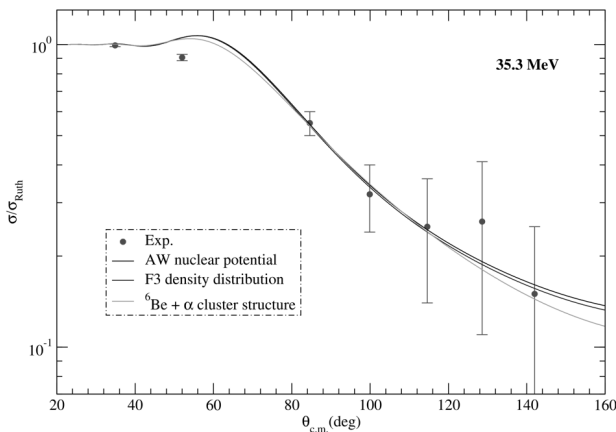


Fig. 7. Comparison of the best results achieved from the nuclear potentials, density distributions, and cluster analysis of the ${}^{10}\text{C} + {}^{58}\text{Ni}$ reaction

Table 6. The normalization constant (N_R), WS parameters, and $\frac{\chi^2}{N}$ values for the calculations with ${}^6\text{Be} + \alpha$, ${}^9\text{B} + p$ and ${}^8\text{Be} + 2p$

Cluster type	N_R	W_0 , MeV	r_w , fm	a_w , fm	$\frac{\chi^2}{N}$
${}^6\text{Be} + \alpha$	1.00	32.9	1.42	0.340	1.80
${}^9\text{B} + p$	0.70	20.0	1.42	0.235	1.83
${}^8\text{Be} + 2p$	0.50	20.0	1.42	0.235	1.94

our study. From the comparison of the results for the densities studied for the first time, it was found that F3 result was better than the others. This result is in agreement with the result of Jouanne *et al.* [39]. Based on this common point of Jouanne *et al.* [39] and

our study, we can say that the F3 density distribution is important in the analysis of nuclear interactions of ${}^{10}\text{C}$ nucleus.

6.3. Comparison of simple cluster results

In our work, we also investigated ${}^6\text{Be} + \alpha$, ${}^9\text{B} + p$, and ${}^8\text{Be} + 2p$ cluster structures of ${}^{10}\text{C}$. The calculations based on a simple cluster approach were performed by using the OM with the code FRESKO [51]. Thus, the real potential was got for three cluster configurations of ${}^{10}\text{C}$ nucleus within the DFM with the use of the code DF POT [52]. Additionally, the imaginary part was selected as the WS type, whose parameters were researched at 0.1 and 0.01 step intervals. The values were listed in Table 6.

Figure 6 displays the elastic scattering cross-section of the ${}^{10}\text{C} + {}^{58}\text{Ni}$ system at 35.3 MeV for different cluster structures. It is seen that the ${}^6\text{Be} + \alpha$ result is better than both ${}^9\text{B} + p$ and ${}^8\text{Be} + 2p$ cluster results. We would like to express that the results mentioned for cluster states of ${}^{10}\text{C}$ here are not certain, but it is purposed to giving a different deepness to future works.

Guimaraes *et al.* [3] performed a simplified CDCC calculation with a three-body configuration for the ${}^9\text{B} + p$ or ${}^6\text{Be} + \alpha$ cluster in order to check the importance of the breakup channels for ${}^{10}\text{C} + {}^{58}\text{Ni}$ in their work. They reported that ${}^9\text{B} + p$ gives a quite good description of the cross sections at backward angles, although ${}^6\text{Be} + \alpha$ is found to be less important. As the reason for this, they stated that ${}^6\text{Be} + \alpha$ has a higher breakup energy ($S_\alpha = 5.101$ MeV) compared to the ${}^9\text{B} + p$ channel ($S_p = 4.006$ MeV). In addition, both we and they indicated that the results regarding the cluster status of ${}^{10}\text{C}$ nucleus are not certain. As a result of all, we would like to state that more studies with different approaches regarding the cluster status of ${}^{10}\text{C}$ nucleus are needed.

6.4. Simultaneous comparison of nuclear potential, density distribution and cluster results

Here, we compare the best results for different nuclear potentials, different density distributions, and different cluster structures, which are AW potential, F3 density, and the ${}^6\text{Be} + \alpha$ cluster state, respectively. As will be seen from Fig. 7, we can deduce

that AW result is better than the other results. Additionally, we can signify that F3 result is better than the result for the $^6\text{Be} + \alpha$ cluster state. These results can also be verified from the $\frac{\chi^2}{N}$ values.

6.5. Simultaneous comparison of the reaction cross-sections

The cross-section is one of the important parameters known in nuclear interactions. We have given the cross-sections for all the investigated systems in Table 7. They are between 452–580 mb. Similar values of the cross-sections acquired via different theoretical calculations can be based upon the well-defined

Table 7. The cross-sections (in mb) calculated by using Prox 77, Prox 79, Mod-Prox 88, Prox 2003-I, Prox 2003-II, Prox 2010, BW 91, AW 95, AW, CW 76, Bass 80, Ngo 80, and D potentials, VMC, Ngo, G1, G2, SP, F1, F2, F3, F4, and F5 densities, and $^6\text{Be} + \alpha$, $^9\text{B} + p$, and $^8\text{Be} + 2p$ cluster structures

System	σ (mb)
Prox 77	539
Prox 79	514
Mod-Prox 88	487
Prox 2003-I	529
Prox 2003-II	539
Prox 2010	504
BW 91	485
AW 95	505
AW	504
CW 76	496
Bass 80	507
Ngo 80	553
D	580
VMC	473
Ngo	471
G1	513
G2	512
SP	500
F1	480
F2	475
F3	512
F4	477
F5	474
$^6\text{Be} + \alpha$	551
$^9\text{B} + p$	452
$^8\text{Be} + 2p$	453

experimental data. So, it can be drawn a conclusion that the approaches applied in this work are convenient for the $^{10}\text{C} + ^{58}\text{Ni}$ system.

7. Summary and Conclusions

In this work, we firstly obtained the elastic cross-section of the $^{10}\text{C} + ^{58}\text{Ni}$ system for thirteen different nuclear potentials. We have found that AW potential was more effective than the other potentials.

Second, we presented the elastic scattering cross-section for the $^{10}\text{C} + ^{58}\text{Ni}$ system by using ten various densities of ^{10}C . We observed that the consistency with the experimental data of G1, G2, and F3 densities is better than the results for other densities. Additionally, we noticed that F3 density is very slightly better than G1 and G2 densities within the scope of the error value.

Third, we obtained the elastic scattering cross-section of $^{10}\text{C} + ^{58}\text{Ni}$ for $^6\text{Be} + \alpha$, $^9\text{B} + p$, and $^8\text{Be} + 2p$ clusters of ^{10}C . We realized that the $^6\text{Be} + \alpha$ cluster result is better than $^9\text{B} + p$ and $^8\text{Be} + 2p$ cluster results in fitting the experimental data.

Consequently, the present study provides new and useful results such as alternative potential (AW), alternative density (F3), and an alternative computational process of cluster states of ^{10}C . Additionally, we can say that the results obtained for the potential, density distribution and cluster structure of ^{10}C nucleus can be evaluated in the analysis of elastic scattering reactions of ^{10}C with other target nuclei except for ^{58}Ni target nucleus.

The author would like to thank the anonymous referee for valuable comments.

1. <https://www.nndc.bnl.gov/nudat2/>
2. <https://knotplot.com/brunnian/>
3. V. Guimarães, E.N. Cardozo, V.B. Scarduelli, J. Lubian, J.J. Kolata, P.D. O'Malley, D.W. Bardayan, E.F. Aguilera, E. Martinez-Quiroz, D. Lizcano, A. Garcia-Flores, M. Febbraro, C.C. Lawrence, J. Riggins, R.O. Torres-Isea, P.N. de Faria, D.S. Monteiro, E.S. Rossi, Jr., N.N. Deshmukh. Strong coupling effect in the elastic scattering of the $^{10}\text{C} + ^{58}\text{Ni}$ system near barrier. *Phys. Rev. C* **100**, 034603 (2019).
4. G.R. Satchler, W.G. Love. Folding model potentials from realistic interactions for heavy-ion scattering. *Phys. Rep.* **55**, 183 (1979).
5. S.A. Goncharov, A. Izadpanah. Nucleus-nucleus potential within the semi microscopic dispersive model on the basis of a corrected folding-model potential. *Phys. Atom. Nucl.* **70**, 18 (2007).

6. M. Aygun. Alternative potentials analyzing the scattering cross sections of ${}^7,9,10,11,12,14\text{Be}$ isotopes from a ${}^{12}\text{C}$ target: Proximity potentials. *J. Korean Phys. Soc.* **73**, 1255 (2018).
7. M. Aygun. A comparison of proximity potentials in the analysis of heavy-ion elastic cross sections. *Ukr. J. Phys.* **63**, 881 (2018).
8. M. Aygun. The application of some nuclear potentials for quasielastic scattering data of the ${}^{11}\text{Li} + {}^{28}\text{Si}$ reaction and its consequences. *Turk. J. Phys.* **42**, 302 (2018).
9. J. Blocki, J. Randrup, W.J. Swiatecki, C.F. Tsang. Proximity forces. *Ann. Phys. (NY)* **105**, 427 (1977).
10. I. Dutt, R.K. Puri. Comparison of different proximity potentials for asymmetric colliding nuclei. *Phys. Rev. C* **81**, 064609 (2010).
11. W.D. Myers, W.J. Swiatecki. Nuclear masses and deformations. *Nucl. Phys.* **81**, 1 (1966).
12. H.J. Krappe, J.R. Nix, A.J. Sierk. Unified nuclear potential for heavy-ion elastic scattering, fusion, fission, and ground-state masses and deformations. *Phys. Rev. C* **20**, 992 (1979).
13. R. Kumar. Effect of isospin on the fusion reaction cross-section using various nuclear proximity potentials within the Wong model. *Phys. Rev. C* **84**, 044613 (2011).
14. K. Pomorski, J. Dudek. Nuclear liquid-drop model and surface-curvature effects. *Phys. Rev. C* **67**, 044316 (2003).
15. I. Dutt, R.K. Puri. Role of surface energy coefficients and nuclear surface diffuseness in the fusion of heavy-ions. *Phys. Rev. C* **81**, 047601 (2010).
16. R. Gharaei, V. Zanganeh, N. Wang. Systematic study of proximity potentials for heavy-ion fusion cross sections. *Nucl. Phys. A* **979**, 237 (2018).
17. W. Reisdorf. Heavy-ion reactions close to the Coulomb barrier. *J. Phys. G: Nucl. Part. Phys.* **20**, 1297 (1994).
18. G.L. Zhang, Y.J. Yao, M.F. Guo, M. Pan, G.X. Zhang, X.X. Liu. Comparative studies for different proximity potentials applied to large cluster radioactivity of nuclei. *Nucl. Phys. A* **951**, 86 (2016).
19. A. Winther. Dissipation, polarization and fluctuation in grazing heavy-ion collisions and the boundary to the chaotic regime. *Nucl. Phys. A* **594**, 203 (1995).
20. Ö. Akyüz, A. Winter. *Proceedings of the International School of Physics "Enrico Fermi", Course LXXVII, Varenna, Italy, 1979*, Ed. by R.A. Broglia, C.H. Dasso, R. Richi (North-Holland, 1981), p. 492.
21. R.N. Sagaidak, S.P. Tretyakova, S.V. Khlebnikov, A.A. Ogloblin, N. Rowley W.H. Trzaska. Nuclear potentials for sub-barrier fusion and cluster decay in ${}^{14}\text{C}$, ${}^{18}\text{O} + {}^{208}\text{Pb}$ systems. *Phys. Rev. C* **76**, 034605 (2007).
22. P.R. Christensen, A. Winther, The evidence of the ion-ion potentials from heavy ion elastic scattering. *Phys. Lett. B* **65**, 19 (1976).
23. H. Ngô, C. Ngô. Calculation of the real part of the interaction potential between two heavy ions in the sudden approximation. *Nucl. Phys. A* **348**, 140 (1980).
24. V. Yu Denisov. Interaction potential between heavy ions. *Phys. Lett. B* **526**, 315 (2002).
25. M. Aygun. A comprehensive analysis of elastic scattering of ${}^{14}\text{N}$ projectile on ${}^7\text{Li}$, ${}^9\text{Be}$, ${}^{11}\text{B}$, ${}^{12}\text{C}$, ${}^{16}\text{O}$, ${}^{26}\text{Mg}$, ${}^{28}\text{Si}$, ${}^{40}\text{Ca}$, ${}^{56}\text{Fe}$, ${}^{59}\text{Co}$, ${}^{60,62}\text{Ni}$, ${}^{70,74}\text{Ge}$, ${}^{90}\text{Zr}$, ${}^{112}\text{Cd}$, ${}^{118}\text{Sn}$, ${}^{159}\text{Tb}$ and ${}^{197}\text{Au}$ at various incident energies. *Chin. J. Phys.* **55**, 2559 (2017).
26. M. Aygun. Analysis with SDHO and RMF density distributions of elastic scattering cross-sections of oxygen isotopes (${}^{16-18}\text{O}$) by various target nuclei. *Int. J. Mod. Phys. E* **27**, 1850055 (2018).
27. M. Aygun. Double-folding analysis of the ${}^6\text{Li} + {}^{58}\text{Ni}$ reaction using the ab initio density distribution. *Eur. Phys. J. A* **48**, 145 (2012).
28. M. Aygun, Y. Kucuk, I. Boztosun, A.A. Ibraheem. Microscopic few-body and Gaussian-shaped density distributions for the analysis of the ${}^6\text{He}$ exotic nucleus with different target nuclei. *Nucl. Phys. A* **848**, 245 (2010).
29. M. Aygun. A comprehensive description of ${}^{19}\text{F}$ elastic scattering by ${}^{12}\text{C}$, ${}^{16}\text{O}$, ${}^{66}\text{Zn}$, ${}^{159}\text{Tb}$, and ${}^{208}\text{Pb}$ target nuclei. *Braz. J. Phys.* **49**, 760 (2019).
30. T. Ulucay, M. Aygun. A comprehensive description of elastic scattering angular distributions for eight different density distribution of ${}^{32}\text{S}$ nucleus. *Rev. Mex. Fis.* **66**, 336 (2020).
31. <https://www.phy.anl.gov/theory/research/density/>
32. C. Ngô, B. Tamain, M. Beiner, R.J. Lombard, D. Mas, H.H. Deubler. Properties of heavy ion interaction potentials calculated in the energy density formalism. *Nucl. Phys. A* **252**, 237 (1975).
33. R.K. Gupta, D. Singh, W. Greiner. Semiclassical and microscopic calculations of the spin-orbit density part of the Skyrme nucleus-nucleus interaction potential with temperature effects included. *Phys. Rev. C* **75**, 024603 (2007).
34. O.N. Ghodsi, F. Torabi. Comparative study of fusion barriers using Skyrme interactions and the energy density functional. *Phys. Rev. C* **92**, 064612 (2015).
35. R.K. Gupta, D. Singh, R. Kumar, W. Greiner. Universal functions of nuclear proximity potential for Skyrme nucleus-nucleus interaction in a semiclassical approach. *J. Phys. G: Nucl. Part. Phys.* **36**, 075104 (2009).
36. L.C. Chamon, B.V. Carlson, L.R. Gasques, D. Pereira, C. De Conti, M.A.G. Alvarez, M.S. Hussein, M.A. Cândido Ribeiro, E.S. Rossi, Jr., C.P. Silva. Toward a global description of the nucleus-nucleus interaction. *Phys. Rev. C* **66**, 014610 (2002).
37. W.M. Seif, H. Mansour. Systematics of nucleon density distributions and neutron skin of nuclei. *Int. J. Mod. Phys. E* **24**, 1550083 (2015).
38. M. Ismail, W.M. Seif, W.M. Tawfik, A.M. Hussein. Effect of choosing the Q_α -values and daughter density distributions on the magic numbers predicted by α decays. *Ann. Physics* **406**, 1 (2019).
39. C. Jouanne, V. Lapoux, F. Auger, N. Alamanos, A. Drouart, A. Gillibert, G. Lobo, A. Musumarra, L. Nalpas, E. Pollacco, J.-L. Sida, M. Trotta, Y. Blumenfeld, E. Khan, T. Suomijärvi, T. Zerguerras, P. Rousset-Chomaz, H. Savajols, A. Lagoyannis, A. Pakou. Structure

- of low-lying states of $^{10,11}\text{C}$ from proton elastic and inelastic scattering. *Phys. Rev. C* **72**, 014308 (2005).
40. H. Schechter, L.F. Canto. Proximity formulae for folding potentials. *Nucl. Phys. A* **315**, 470 (1979).
 41. S.A. Moszkowski. Energy dependence of the ion-ion potential with a simplified energy density method. *Nucl. Phys. A* **309**, 273 (1978).
 42. M. El-Azab Farid, M.A. Hassanain. Density-independent folding analysis of the $^{6,7}\text{Li}$ elastic scattering at intermediate energies. *Nucl. Phys. A* **678**, 39 (2000).
 43. M. Aygun. A comparative analysis of the density distributions and the structure models of ^9Li . *Pramana – J. Phys.* **88**, 53 (2017).
 44. M. Aygun, Z. Aygun. A theoretical study on different cluster configurations of the ^9Be nucleus by using a simple cluster model. *Nucl. Sci. Tech.* **28**, 86 (2017).
 45. M. Aygun. A comprehensive study on the internal structure and the density distribution of ^{12}Be . *Rev. Mex. Fis.* **62**, 336 (2016).
 46. M. Aygun. A comprehensive theoretical analysis of ^{22}Ne nucleus by using different density distributions, different nuclear potentials and different cluster approach. *Int. J. Mod. Phys. E* **29**, 1950112 (2020).
 47. A.K. Chaudhuri. Density distribution of ^{11}Li and proton elastic scattering from ^9Li and ^{11}Li . *Phys. Rev. C* **49**, 1603 (1994).
 48. R.A. Rego. Closed-form expressions for cross sections of exotic nuclei. *Nucl. Phys. A* **581**, 119 (1995).
 49. R.J. Charity, T.D. Wiser, K. Mercurio, R. Shane, L.G. Sobotka, A.H. Wuosmaa, A. Banu, L. Trache, R.E. Tribble. Continuum spectroscopy with a ^{10}C beam: Cluster structure and three-body decay. *Phys. Rev. C* **80**, 024306 (2009).
 50. A. Ozawa, I. Tanihata, T. Kobayashi, Y. Sugahara, O. Yamakawa, K. Omata, K. Sugimoto, D. Olson, W. Christie, H. Wieman. Interaction cross sections and radii of light nuclei. *Nucl. Phys. A* **608**, 63 (1996).
 51. I.J. Thompson. Coupled reaction channels calculations in nuclear physics. *Comput. Phys. Rep.* **7**, 167 (1988).
 52. J. Cook. DF POT – A program for the calculation of double folded potentials. *Commun. Comput. Phys.* **25**, 125 (1982).

Received 15.09.20

M. Айзун

ПОВНЕ ДОСЛІДЖЕННЯ ЯДРА ^{10}C З ВИКОРИСТАННЯМ РІЗНИХ ТЕОРЕТИЧНИХ ПІДХОДІВ

Виконано детальний теоретичний аналіз властивостей ядра ^{10}C із застосуванням різних теоретичних підходів для різних ядерних потенціалів і розподілів густини на основі простої кластерної моделі. Ми спробували пояснити нові незрозумілі експерименти для системи $^{10}\text{C} + ^{58}\text{Ni}$ при 35,3 МеВ. Спочатку ми розглянули 13 різних потенціалів, а потім 10 різних типів розподілу густини для ядра ^{10}C . Запропоновано простий метод розрахунку кластерних станів ядра ^{10}C . Проведено порівняння всіх теоретичних результатів з експериментальними даними і досягнуто їх краще узгодження.

Ключові слова: ядерний потенціал, потенціал близькодії, розподіл густини, кластерна модель, пружне розсіяння, оптична модель, модель подвійної згортки.